

COVER PAGE

Document downloaded by @DAEL

Thu Nov 26 19:41:01 2026
For personal use

When automatic English translation is provided, only the original document is authentic.
The EAA cannot be held responsible of any translation error

Bibliographical reference

The Parallel Solution of Discrete Linearized Navier–Stokes Equations in the Frequency Domain, Mika Malinen, Juha Ruokolainen and Peter Råback, Acta Acustica **vol. 100** (Number 1), 2014, pp. 102-112

DOI
https://doi.org/10.3813/AAA.918690

Acta Acustica united with Acustica
Vol. 100 (2014) 102 – 112

DOI 10.3813/AAA.918690

The Parallel Solution of Discrete Linearized Navier–Stokes Equations in the Frequency Domain

Mika Malinen, Juha Ruokolainen, Peter Råback
CSC - IT Center for Science Ltd., P.O. Box 405, 02101 Espoo, Finland. mika.malinen@csc.fi

Summary
An effective computational strategy for handling the finite element version of linearized Navier–Stokes equations in the frequency domain is described. The coupled linear systems resulting from applying this computational model to acoustical problems are typically very large and difficult to solve with standard preconditioned linear solvers. Emphasis is therefore placed on deriving an alternate formulation of the governing equations with the efficient utilization of parallel computers in mind. The treatment given highlights that this goal is intimately related to deriving an effective block preconditioning strategy where the action of the preconditioner depends on solving simple auxiliary problems. The utility of the solver described is demonstrated computationally by using representative small-amplitude acoustics problems, including large cases posed on three-dimensional bodies.

PACS no. 43.20.-f, 43.20.Hq

1. Introduction

The acoustic wave motion in a viscous and thermally diffusive fluid obeying the perfect gas law can be characterized by the time-harmonic version of linearized Navier–Stokes equations. These equations may be written in a dimensionless form as

$$\begin{aligned} \theta \mathbf{v}' + \frac{\mathrm{i}}{Re}\Delta'\mathbf{v}' + \frac{\mathrm{i}}{Re}(1+\eta)\nabla'(\nabla'\cdot\mathbf{v}') - \mathrm{i}\nabla' p' &= \mathbf{0}, \\ -\frac{\mathrm{i}}{Pe}\Delta'\tau' - \theta\tau' + \theta p' &= 0, \\ \mathrm{i}\nabla'\cdot\mathbf{v}' + (\gamma-1)\theta\tau' - \gamma\theta p' &= 0, \end{aligned} \tag{1}$$

with the complex-valued fields $\mathbf{v}'(\mathbf{x}')$, $p'(\mathbf{x}')$ and $\tau'(\mathbf{x}')$ giving the amplitudes of velocity, pressure and temperature fluctuations about an equilibrium state, respectively. Here the dimensionless variables have been obtained by introducing dimensionless place $\mathbf{x}' = \mathbf{x}/L$ and time $t' = \omega t$, with ω the angular frequency and L a typical length characterizing the size of the body considered (the use of the dimensionless place also leads to denoting the gradient and Laplacian operators with respect to $\mathbf{x}'$ by ∇' and $\mathbf{\Delta}'$, respectively). By letting $\gamma = C_P/C_V$ to be the ratio of specific heats at constant pressure and at constant volume, we have also selected the characteristic values of the velocity, pressure and temperature to be $V = c$, $P = \rho_0 c^2$ and $T = (\gamma - 1)T_0$, with c the adiabatic sound speed, ρ_0 the equilibrium density and T_0 the equilibrium temperature. The characteristic numbers appearing in (1) are then the Strouhal number $\theta = \omega L/V$, the Reynolds number $Re = \rho_0 V L/\mu$, and the Peclet number $Pe = \rho_0 C_p V L/K$, where μ and K are the dynamic viscosity and thermal conductivity, respectively. Finally, the value of the other viscosity parameter η depends on the bulk viscosity κ of the fluid as $\eta = \kappa/\mu - 2/3$.

The model (1) has a wide range of applicability in small-amplitude acoustics. Its principal limitation is the assumed linearity, so that the nonlinear terms in the underlying full Navier–Stokes equations can be neglected. This can be shown to be a feasible approximation when the Mach number is small, i.e. when $\epsilon = |V\mathbf{v}'|/c = |\mathbf{v}'| \ll 1$. More approximate models which are common in practice may also be obtained from (1) by introducing further simplifications. For example, by neglecting the dissipative effects of viscosity and thermal diffusion we come to the standard Helmholtz model. However, an accurate description of wave propagation may require that all terms in (1) are well approximated. Examples of such situation are the wave propagation in narrow ducts and the condition of resonance.

The finite element method offers direct ways to approximate solutions to the linearized Navier–Stokes model (1) computationally, and the development and application of such methods have received growing interest in recent years; cf. [1, 2, 3, 4]. A strength of these methods is that they offer the possibility of handling general problem geometries in a conceptually straightforward manner. In addition, they do not involve additional modelling errors which relate to simplifying the model (1). While the goal of such simplifications is usually to improve the computational efficiency, the downside is that the validity regimes

Received 28 February 2013,
accepted 12 November 2013.

© S. Hirzel Verlag · EAA

of resulting models may not be clear always. However, by adopting the use of the linearized Navier–Stokes model, the analyst does not need to be equally concerned about the limitations of the model employed.

The essential challenges in the finite element approximation of (1) are related to the nearly incompressible behaviour of solutions when the parameter θ is small, the multiscale nature of solutions, and the strong physical coupling of the constituent solution fields. We note that the desirability of robust solution methods with respect to variations of θ prevents the straightforward approximation of (1) by using standard equal-order interpolation elements and, similarly, hinder the approximation of the associated set of reduced equations in the velocity and temperature variables with low-order elements (hence, we do not recommend using a low-order approximation of the formulation employed in [3]; see [1] for an original discussion of this point and, also, [5, 6] for additional experimental evidence). On the other hand, the multiscale nature relates to the presence of rapidly decaying solution components which are negligible outside thin boundary layers. Obtaining high-quality discrete approximations therefore requires the use of carefully refined discretizations in the boundary layers. This easily leads to very large linear systems, especially, in the case of three-dimensional bodies. Thus, in order for this model to have utility in a practical design environment, robust and efficient iterative linear solvers which are able to treat the strong physical coupling of the fields are needed. It is also noted that handling large discrete problems almost certainly requires the utilization of parallel computers, so these solution methods should also be developed with this option in mind.

If we now scale the dimensionless heat equation, i.e. the second equation in the system (1), by multiplying with a quantity $\gamma - 1$, the finite element methods which treat the resulting coupled equations directly lead typically to solving a linear algebra problem

$$\begin{bmatrix} \mathbf{A} & \mathbf{0} & \mathbf{B}^T \\ \mathbf{0} & \mathbf{J} & \mathbf{D} \\ \mathbf{B} & \mathbf{D} & \mathbf{C} \end{bmatrix} \begin{bmatrix} \mathbf{V} \\ \mathbf{T} \\ \mathbf{P} \end{bmatrix} = \begin{bmatrix} \mathbf{F} \\ \mathbf{0} \\ \mathbf{0} \end{bmatrix}, \tag{2}$$

where the complex symmetric coefficient matrix is of the form $\mathbf{K} = \mathbf{G} + i\mathbf{H}$, with both $\mathbf{G}$ and $\mathbf{H}$ real and indefinite (some linear solvers make use of complex symmetry which motives the scaling considered, cf. [2]). Perhaps the most promising iterative methods for solving the coupled system (2) are based on the Schur complement reduction. The elimination of the velocity unknowns $\mathbf{V}$ from the discrete continuity equation, the continuous version of which is the last equation in (1), leads us to an equivalent problem

$$\begin{bmatrix} \mathbf{A} & \mathbf{0} & \mathbf{B}^T \\ \mathbf{0} & \mathbf{J} & \mathbf{D} \\ \mathbf{0} & \mathbf{D} & \mathbf{S} \end{bmatrix} \begin{bmatrix} \mathbf{V} \\ \mathbf{T} \\ \mathbf{P} \end{bmatrix} = \begin{bmatrix} \mathbf{F} \\ \mathbf{0} \\ -\mathbf{B}\mathbf{A}^{-1}\mathbf{F} \end{bmatrix}, \tag{3}$$

with $\mathbf{S} = \mathbf{C} - \mathbf{B}\mathbf{A}^{-1}\mathbf{B}^T$. This problem formulation decouples the solution of the velocity from that of the temperature and pressure vectors $\mathbf{T}$ and $\mathbf{P}$. Although the direct utilization of the formulation (3) is not realistic due to the need of computing the inverse $\mathbf{A}^{-1}$, many stationary as well as preconditioned Krylov iteration methods can be either derived from or intimately related to the formulation (3); cf. the monograph [7], which treats analogous problems by restricting to real coefficient matrices. Common to all these methods is that their performance depends crucially on the quality of an approximation to the coefficient matrix associated with the Schur complement problem

$$\begin{bmatrix} \mathbf{J} & \mathbf{D} \\ \mathbf{D} & \mathbf{C} - \mathbf{B}\mathbf{A}^{-1}\mathbf{B}^T \end{bmatrix} \begin{bmatrix} \mathbf{T} \\ \mathbf{P} \end{bmatrix} = \begin{bmatrix} \mathbf{0} \\ -\mathbf{B}\mathbf{A}^{-1}\mathbf{F} \end{bmatrix} \tag{4}$$

embedded in the formulation (3).

To understand practical difficulties which relate to approximating the Schur complement problem (4) in a consistent manner, it is worthwhile to note that the elimination procedure similar to that presented above can already be done for the continuous problem by employing the Helmholtz decomposition. Eliminating the velocity $\mathbf{v}'$ from the continuity equation then leads us to the weak formulation of an associated pressure equation which states that the weak solution of the problem satisfies

$$\begin{aligned} &-\frac{\mathrm{i}(2+\eta)(\gamma-1)}{Re}\left\langle \nabla'\tau', \nabla' q' \right\rangle \\ &+\frac{1}{\theta}\left[1+\frac{\mathrm{i}(2+\eta)\theta\gamma}{Re}\right]\left\langle \nabla' p', \nabla' q' \right\rangle \\ &+(\gamma-1)\theta\left\langle \tau', q' \right\rangle \\ &-\gamma\theta\left\langle p', q' \right\rangle = -\mathrm{i}\left\langle \mathbf{w}'\cdot\mathbf{e}_{n'}, q' \right\rangle_{\partial\Omega'} \end{aligned} \tag{5}$$

for all $q' \in H^1(\Omega')$. Here $\langle \cdot, \cdot \rangle$ denotes L_2 inner product, with the domain of integration indicated with a subscript if different from the d-dimensional body Ω' on which the problem is posed. In addition, $\mathbf{e}_{n'}$ is the outward unit normal to the boundary $\partial\Omega'$ of Ω' and $\mathbf{w}'$ is the irrotational part of the velocity solution in the unique splitting of the velocity into the solenoidal and irrotational parts as $\mathbf{v}' = \mathbf{u}' + \mathbf{w}'$.

In essence, the pressure equation corresponding to (5) together with the heat equation characterize the solution in a nearly similar manner as the discrete Schur complement problem (4) does. However, the principal difficulty in utilizing (5) is that the associated consistent boundary condition depends on the part $\mathbf{w}'$ which is unknown until the solution is found. Moreover, if we circumvent this difficulty by seeking the solution iteratively, there is an additional burden in representing the consistent boundary condition as the field $\mathbf{w}'$ is not computed automatically when the equations are treated in the form (1). Although the discrete alternate (4) seems to avoid these problems as the associated boundary conditions are in-built into the discrete equations, in practice it is far from clear how an approximation of (4) should be constructed so that the in-built constraints are respected faithfully. Since the continuous pressure equation corresponding to (5) gives us a definite description on what needs to be specified on the boundary in order to decouple the solution of the pressure and temperature from that of the velocity, we have previously

come to prefer the above continuous version of the Schur complement reduction as a starting point for developing block triangular preconditioners for Krylov methods. For a practical preconditioned iteration method that is essentially based on the idea of the consistent approximation of (5) see [8].

Although the preconditioned Krylov solvers based on approximating the block triangular system relating to the Schur complement reduction are very promising in the sense that they may exhibit convergence rates which do not depend on the problem size, their efficient implementation and paralleling in connection with the linearized Navier–Stokes model considered form an open issue. We note that here the associated Schur complement problem yet couples the solution of the pressure and temperature in a strong manner and may also be ill-conditioned. For efficiency it would be desirable to employ a splitting strategy that leads to a block preconditioner whose action can be computed by solving simple scalar equations independently. In this paper, emphasis is placed on deriving an alternate formulation of the problem (1) that is better compatible with this goal.

The remainder of this paper is organized as follows. In Section 2 we derive the system of split equations which forms a basis for an alternate finite element approximation of the model (1). The techniques we employ in the derivation are mainly classic, being based on the use of the Helmholtz decomposition. A simple change of variables is additionally introduced in order to weaken the coupling of the resulting equations. We note that at the first glance the use of the alternate formulation in the finite element approximation seems to lead to a considerable overhead in the computation. Fortunately, there exist effective ways to handle the solution of the resulting linear algebra problem with Krylov methods which employ a sparse representation of the associated search space in conjunction with the block Gauss-Seidel preconditioning. Section 3 is devoted to describing this methodology. Finally, in Section 4, the practical utility of the ideas is shown. We present computational experiments which demonstrate the optimal accuracy of the alternate discrete model to describe the solutions of the model (1) as the discretization is refined. Generally, these computations as well as all other experiments performed demonstrate rapid convergence of the preconditioned iterative solver we propose. Importantly, the feasibility of parallel computing in conjunction with the proposed solution strategy is also shown by considering the parallel solution of high-fidelity approximation in the case of a Helmholtz resonator model in three dimensions.

2. Splitting strategy

The splitting strategies utilized in this section are mainly based on the classic idea of employing the Helmholtz decomposition, the acoustic applications of which are well described in the literature; see, eg., [9, Section 6.4]. At the cost of introducing additional variables the problem (1) may thus be reformulated as a coupled system of simpler equations. As mentioned in the introduction, the desirability of obtaining such simplicity is indeed central to our approach. Later sections of this paper will then be devoted to describing how these equations can be employed in practice to produce computational solutions which faithfully approximate the solution to the original system (1).

We note that by employing the Helmholtz decomposition $\mathbf{v}' = \mathbf{u}' + \mathbf{w}'$, with $\mathbf{u}'$ solenoidal and $\mathbf{w}'$ irrotational, the original field equations separate into the two sets of equations

$$\begin{aligned} \theta\mathbf{w}' + \frac{\mathrm{i}}{Re}(2+\eta)\nabla'(\nabla'\cdot\mathbf{w}') - \mathrm{i}\nabla' p' &= \mathbf{0}, \\ -\frac{\mathrm{i}}{Pe}\Delta'\tau' - \theta\tau' + \theta p' &= 0, \\ \mathrm{i}\nabla'\cdot\mathbf{w}' + (\gamma-1)\theta\tau' - \gamma\theta p' &= 0 \end{aligned} \tag{6}$$

and

$$\theta\mathbf{u}' - \frac{\mathrm{i}}{Re}\nabla'\times\nabla'\times\mathbf{u}' = \mathbf{0}. \tag{7}$$

By eliminating $\mathbf{w}'$, the system (6) then yields the continuous version of the Schur complement equations

$$\begin{aligned} -\frac{\mathrm{i}}{Pe}\Delta'\tau' - \theta\tau' + \theta p' &= 0, \\ \frac{(2+\eta)\mathrm{i}}{Re}\left[(\gamma-1)\Delta'\tau' - \gamma\Delta' p'\right] & \\ -\frac{1}{\theta}\Delta' p' + (\gamma-1)\theta\tau' - \gamma\theta p' &= 0, \end{aligned} \tag{8}$$

with $\mathbf{w}'$ found after solving for τ' and p' from

$$\theta\mathbf{w}' - \frac{2+\eta}{Re}\nabla'\left[(\gamma-1)\theta\tau' - \gamma\theta p'\right] - \mathrm{i}\nabla' p' = \mathbf{0}. \tag{9}$$

The systems (6) and (7) are basically coupled only by their boundary conditions. It should be noted that the system (7) admits specifying its boundary conditions only in the tangential directions to the boundary. In contrast, the normal component of $\mathbf{w}'$ can be specified in connection with handling (6). Thus, in cases where the boundary conditions are of the Dirichlet type

$$\mathbf{v}' = \mathbf{g}' \quad \text{and} \quad \tau' = 0, \tag{10}$$

with $\mathbf{g}'$ given on the boundary, the part $\mathbf{u}'$ must satisfy the tangential constraint

$$\mathbf{e}_{n'}\times\mathbf{u}'\times\mathbf{e}_{n'} = \mathbf{e}_{n'}\times\mathbf{g}'\times\mathbf{e}_{n'} - \mathbf{e}_{n'}\times\mathbf{w}'\times\mathbf{e}_{n'}. \tag{11}$$

On the other hand, the velocity constraint associated with (6) is

$$\mathbf{w}'\cdot\mathbf{e}_{n'} = \mathbf{g}'\cdot\mathbf{e}_{n'} - \mathbf{u}'\cdot\mathbf{e}_{n'}. \tag{12}$$

We note that, in view of (5) which is the weak formulation of the second equation in (8), the constraint (12) can be built easily into the weak formulation of the reduced system (8).

The utility of the split system consisting of (7), (8) and (9) is still constrained by the fact that the computational solution of (8) is not particularly easy. It nevertheless appears that a simple change of variables described next can be helpful.

It turns out that under the common condition $\theta/Pe \ll 1$ and $\theta/Re \ll 1$ the temperature solution outside the boundary layer may be approximated as $\tau' = p'$. It is therefore natural to consider constructing the temperature solution as

$$\tau' = p' + \vartheta', \tag{13}$$

so that the new variable ϑ' basically plays the role of an edge correction to the solution. By using the variables $\mathbf{v}artheta'$ and p', the Schur complement equations (8) can then be rewritten as

$$\begin{aligned} -\frac{\mathrm{i}}{Pe}\Delta'\vartheta' - \theta\vartheta' - \frac{\mathrm{i}}{Pe}\Delta' p' &= 0, \\ \frac{(2+\eta)\mathrm{i}}{Re}\left[(\gamma-1)\Delta'\vartheta' - \Delta' p'\right] - \frac{1}{\theta}\Delta' p' & \\ -\theta p' + (\gamma-1)\theta\vartheta' &= 0. \end{aligned} \tag{14}$$

In order to understand the essential features of (14), we temporarily admit errors which result from simplifying coefficients by neglecting terms of $O(\theta/Re)$ or $O(\theta/Pe)$ in comparison to the unity. Then the set (14) reduces to

$$-\frac{\mathrm{i}}{Pe}\Delta'\vartheta' - \theta\vartheta' + \left(\frac{\mathrm{i}\theta}{Pe}\right)\theta p' = 0, \tag{15}$$

$$-\left[1-(2+\eta)Pr\right](\gamma-1)\frac{\mathrm{i}\theta}{Pe}\Delta'\vartheta' - \Delta' p' - \theta^2 p' = 0, \tag{16}$$

with $Pr = Pe/Re$ the Pradtl number. We now see that the coupling terms in the field equations (15) are relatively weak, as they involve a multiplication with a small factor θ/Pe. The leading parts of ϑ' and p' are thus characterized by the homogeneous diffusion equation

$$-\frac{\mathrm{i}}{Pe}\Delta'\vartheta' - \theta\vartheta' = 0$$

and the Helmholtz equation

$$-\Delta' p' - \theta^2 p' = 0,$$

with the boundary conditions deduced from the relations

$$\vartheta' = \tau' - p'$$

and

$$\nabla' p' \cdot \mathbf{e}_{n'} = -\mathrm{i}\theta\left(\mathbf{g}' \cdot \mathbf{e}_{n'} - \mathbf{u}' \cdot \mathbf{e}_{n'}\right).$$

In essence, the above development reveals that the change of variables via (13) opens up the possibility of solving the Schur complement equations iteratively by reusing solvers for the standard diffusion equation and the Helmholtz equation. On the other hand, the other equations corresponding to the splitting considered have already been found to be standard by their nature. We note that the system (7) characterizing the viscous diffusion process produces a rapidly decaying solution component which is important only in the boundary layer, while (9) can easily be used to generate $\mathbf{w}'$ for given pressure and temperature fields.

Before we proceed to describe how the above equations can be used in practice in the computational solution, we consider an alternate way to formulate (7). This alternate may have merit in connection with the finite element approximation due to the associated simplicity of prescribing boundary conditions.

We note that, depending on the maturity of available finite element software, there may be an additional technicality associated with handling the tangential constraints (11). This issue can nevertheless be avoided if we express the solenoidal part as the curl of a vector potential $\boldsymbol{\psi}'$, so that

$$\mathbf{u}' = \nabla' \times \boldsymbol{\psi}', \tag{17}$$

with an additional constraint $\nabla' \cdot \boldsymbol{\psi}' = 0$. It can be verified that $\boldsymbol{\psi}'$ satisfies the same field equation as $\mathbf{u}'$, i.e.

$$\theta\boldsymbol{\psi}' - \frac{\mathrm{i}}{Re}\nabla' \times \nabla' \times \boldsymbol{\psi}' = \mathbf{0}, \tag{18}$$

so that multiplication with a test function $\boldsymbol{\eta}'$ and integration by parts then give the weak version

$$\begin{aligned} &\theta\left\langle \boldsymbol{\psi}', \boldsymbol{\eta}' \right\rangle - \frac{\mathrm{i}}{Re}\left\langle \nabla' \times \boldsymbol{\psi}', \nabla' \times \boldsymbol{\eta}' \right\rangle \\ &= -\frac{\mathrm{i}}{Re}\left\langle \mathbf{e}_{n'} \times \left(\nabla' \times \boldsymbol{\psi}'\right) \times \mathbf{e}_{n'}, \mathbf{e}_{n'} \times \boldsymbol{\eta}' \right\rangle_{\partial\Omega'}. \end{aligned}$$

We now see that the tangential velocity can be specified as a natural boundary condition in the weak formulation, as we have

$$\mathbf{e}_{n'} \times \left(\nabla' \times \boldsymbol{\psi}'\right) \times \mathbf{e}_{n'} = \mathbf{e}_{n'} \times \mathbf{u}' \times \mathbf{e}_{n'}.$$

After solving for $\boldsymbol{\psi}'$ we may finally generate the solenoidal velocity via (17).

3. The fully coupled solution of the split equations

The idea of generating solutions to the linearized Navier–Stokes model via solving simpler equations is by no manner of means new. Starting from this idea, simple methods have been proposed to provide approximate solutions to the equations which are equivalent to (1); cf. [10, 11] for early computational methods, and [12] and the references therein for later developments. However, a typical drawback of these methods is that their applicability may be limited by additional constraints regarding the problem geometry. In addition, these simplified solution procedures do not use iterative improvement. As a result, they do not provide means of finding finite element solutions of (1) which generally are as accurate as possible relative to the attainable approximation error in the finite element expansion but involve additional modelling errors that are not rigorously controlled. In contrast, the process of iterative improvement is focal to the approach we shall consider here. Thus, we are able to seek for the mathematical solution of the original model (1) iteratively while utilizing the decoupled equations in the iterative solution procedure.

3.1. Weak formulation

We begin the development of computational solution methods by transforming the central equations back into the dimensional form and by writing the weak formulation of the resulting equations. We change our notation accordingly, so that all derivatives will now be with respect to the dimensional coordinates. We first assume that the boundary conditions correspond to the wall conditions (10) and postpone the consideration of other constraints until the end of this section.

By defining $M = H^1(\Omega)$, the weak formulation of the dimensional version of the pressure equation may be expressed as follows: Find $p \in M$ such that

$$\begin{aligned}&\big\langle \nabla p, \nabla q\big\rangle - \Big(\frac{\omega}{c}\Big)^2 \big\langle p, q\big\rangle + \frac{\mathrm{i}(2+\eta)\theta}{Re}\langle \nabla p, \nabla q\rangle \\ &\quad - \frac{\mathrm{i}(2+\eta)\theta}{Re}(\gamma-1)\rho_0 c^2 \big\langle \nabla\vartheta', \nabla q\big\rangle \\ &\quad + (\gamma-1)\rho_0 c^2 \Big(\frac{\omega}{c}\Big)^2 \big\langle \vartheta', q\big\rangle \\ &= -\mathrm{i}\rho_0\omega \big\langle \mathbf{g}\cdot\mathbf{e}_n - \mathbf{u}\cdot\mathbf{e}_n, q\big\rangle_{\partial\Omega}\end{aligned} \tag{19}$$

for any $q \in M$. On the other hand, the dimensionless temperature correction $\vartheta' \in X$ is characterized by the requirement that

$$\begin{aligned}-\frac{\mathrm{i}K}{\rho_0\omega C_p}\Big[\frac{1}{\rho_0 c^2}\big\langle \nabla p, \nabla r\big\rangle + \big\langle \nabla\vartheta', \nabla r\big\rangle\Big] \\ + \big\langle \vartheta', r\big\rangle = 0\end{aligned} \tag{20}$$

for any $r \in H_0^1(\Omega)$. The dimensional temperature τ and pressure p being related by

$$\frac{\tau}{(\gamma-1)T_0} = \frac{p}{\rho_0 c^2} + \vartheta',$$

in the case of the homogeneous boundary condition for the temperature fluctuation the solution space $X \subset H^1(\Omega)$ has to be constructed such that the constraint

$$\vartheta' = -\frac{p}{\rho_0 c^2} \tag{21}$$

is respected (this will be easy, since in practice we shall solve (19) and (20) sequentially). By defining

$$Q = H(\mathrm{div};\Omega) \cap H(\mathrm{curl};\Omega)$$

the irrotational velocity is then characterized by the condition that $\mathbf{w} \in Q$ must satisfy

$$\begin{aligned}\rho_0\omega\langle \mathbf{w}, \mathbf{z}\rangle = \mathrm{i}\big\langle \nabla p, \mathbf{z}\big\rangle - \frac{(2+\eta)\theta}{Re}\big\langle \nabla p, \mathbf{z}\big\rangle \\ + \frac{(2+\eta)\theta}{Re}(\gamma-1)\rho_0 c^2 \big\langle \nabla\vartheta', \mathbf{z}\big\rangle\end{aligned} \tag{22}$$

for any $\mathbf{z} \in Q$.

By writing now

$$\mathbf{u} = \nabla\times\boldsymbol{\psi}$$

for the solenoidal part of the dimensional velocity, the vector potential $\boldsymbol{\psi} \in Q$ can be found by requiring that

$$\begin{aligned}&\big\langle \boldsymbol{\psi}, \boldsymbol{\eta}\big\rangle - \frac{\mathrm{i}\mu}{\rho_0\omega}\big\langle \nabla\times\boldsymbol{\psi}, \nabla\times\boldsymbol{\eta}\big\rangle \\ &= -\frac{\mathrm{i}\mu}{\rho_0\omega}\big\langle \mathbf{e}_n\times(\mathbf{v}-\mathbf{w})\times\mathbf{e}_n, \mathbf{e}_n\times\boldsymbol{\eta}\big\rangle_{\partial\Omega}\end{aligned} \tag{23}$$

for any $\boldsymbol{\eta} \in Q$. Finally, the solenoidal velocity is characterized by the following weak formulation: Find $\mathbf{u} \in Q$ such that

$$\big\langle \mathbf{u}, \boldsymbol{\xi}\big\rangle = \big\langle \nabla\times\boldsymbol{\psi}, \boldsymbol{\xi}\big\rangle \tag{24}$$

for any $\boldsymbol{\xi} \in Q$.

We close this section by noting that it is not difficult to extend the above weak formulations in order to handle other boundary conditions. For example, the problems involving symmetries can be treated by augmenting the variational formulations (19) and (20) by homogeneous natural boundary conditions (corresponding to $\mathbf{w}\cdot\mathbf{e}_n = 0$ and $\nabla\vartheta'\cdot\mathbf{e}_n = 0$) on the part of the boundary where the symmetry condition is imposed. In addition, the homogeneous constraints of Dirichlet type may then be imposed on the tangential components of the vector potential $\boldsymbol{\psi}$ in order to enforce the symmetry requirement $\mathbf{u}\cdot\mathbf{e}_n = (\nabla\times\boldsymbol{\psi})\cdot\mathbf{e}_n = 0$. Another set of useful boundary conditions is given by

$$\begin{aligned}&\nabla p\cdot\mathbf{e}_n = \frac{\mathrm{i}\omega\rho_0}{Z}p, \quad \nabla\vartheta'\cdot\mathbf{e}_n = 0, \\ \text{and}\quad &\mathbf{e}_n\times\big(\mathbf{v}-\mathbf{w}\big)\times\mathbf{e}_n = \mathbf{0},\end{aligned} \tag{25}$$

where Z is a given specific acoustic impedance. These constraints can be used to handle open boundary conditions on parts which are far enough from solid walls, so that the flow can be considered to be potential. They again lead to using homogeneous natural boundary conditions in combination with augmenting the pressure equation formulation by the standard Robin boundary condition.

3.2. Solving the discrete equations

The Galerkin finite element approximation of the weak formulations associated with (19), (20), and (22)–(24) leads to solving coupled linear systems of the form

$$\begin{bmatrix} \mathbf{C} & \mathbf{D} & \mathbf{0} & \mathbf{0} & \mathbf{L}_U \\ \mathbf{E} & \mathbf{J} & \mathbf{0} & \mathbf{0} & \mathbf{0} \\ \mathbf{H}_P & \mathbf{H}_\theta & \mathbf{M}_W & \mathbf{0} & \mathbf{0} \\ \mathbf{0} & \mathbf{0} & \mathbf{L}_W & \mathbf{R} & \mathbf{0} \\ \mathbf{0} & \mathbf{0} & \mathbf{0} & \mathbf{N} & \mathbf{M}_U \end{bmatrix} \begin{bmatrix} \mathbf{P} \\ \boldsymbol{\Theta} \\ \mathbf{W} \\ \mathbf{Q} \\ \mathbf{U} \end{bmatrix} = \begin{bmatrix} \mathbf{G} \\ \mathbf{0} \\ \mathbf{0} \\ \mathbf{F} \\ \mathbf{0} \end{bmatrix}, \tag{26}$$

with the vectors $\mathbf{P}$, $\boldsymbol{\Theta}$, $\mathbf{W}$, $\mathbf{Q}$, and $\mathbf{U}$ giving the complex coefficients in the finite element expansions of p, ϑ', $\mathbf{w}$, $\boldsymbol{\psi}$, and $\mathbf{u}$, respectively. Although the splitting considered enables us to express the linearized Navier–Stokes model in terms of simpler equations, there seems to be a significant overhead in utilizing the discrete version of the split equations as written in (26). Fortunately, there are effective ways to perform the fully coupled solution of (26) without

making the literal assembly of the coupled system. We describe our methodology in this section.

To start with, we note that the block Gauss-Seidel iteration for (26) can be implemented in a memory efficient manner. In this connection, the linear solves associated with the coefficient matrices $\mathbf{M}_W$ and $\mathbf{M}_U$ can be done componentwise and thus require allocating only the scalar velocity mass matrix, which is then utilized sequentially. In addition, the coupling matrices $\mathbf{L}_U$ and $\mathbf{L}_W$ are very sparse as they arise from integration over the boundary. We therefore conclude that the memory requirements for performing the block Gauss-Seidel iteration are not significantly different in comparison with a similar stationary iteration for the system which arises from using the original formulation in the velocity, temperature and pressure variables. Moreover, the possibility of developing a highly efficient implementation emerges since existing solvers for approximating the actions of the inverses of both the scalar mass matrix and the matrices associated with discrete Helmholtz and diffusion problems may be reused in the computation of Gauss-Seidel updates. Despite these merits, our experience on using the block Gauss-Seidel iteration for (26) is that divergence is likely to occur when the problem setup corresponds to finding the system response at resonance. Finding an effective relaxation strategy to enable convergence in such situations has also proved to be a difficult task.

It therefore appears that the block Gauss-Seidel scheme can be utilized better as a preconditioner for a minimal residual iteration applied to the fully coupled problem (26). That is, if we abbreviate the system (26) as

$$\mathbf{K}\mathbf{x} = \mathbf{b}, \tag{27}$$

then, given the previous iterate $\mathbf{x}^{(k)}$, we consider solving a new solution candidate $\hat{\mathbf{x}}^{(k+1)}$ from

$$\mathsf{P}\hat{\mathbf{x}}^{(k+1)} = \mathbf{b} - \big(\mathbf{K} - \mathsf{P}\big)\mathbf{x}^{(k)},$$

with P the block Gauss-Seidel iteration matrix

$$\mathsf{P} = \begin{bmatrix} \mathbf{C} & \mathbf{0} & \mathbf{0} & \mathbf{0} & \mathbf{0} \\ \mathbf{E} & \mathbf{J} & \mathbf{0} & \mathbf{0} & \mathbf{0} \\ \mathbf{H}_P & \mathbf{H}_\theta & \mathbf{M}_W & \mathbf{0} & \mathbf{0} \\ \mathbf{0} & \mathbf{0} & \mathbf{L}_W & \mathbf{R} & \mathbf{0} \\ \mathbf{0} & \mathbf{0} & \mathbf{0} & \mathbf{N} & \mathbf{M}_U \end{bmatrix}, \tag{28}$$

and computing the minimal residual update by using the search direction $\mathbf{s}^{(k+1)} = \hat{\mathbf{x}}^{(k+1)} - \mathbf{x}^{(k)}$. We are thus producing a sequence of improving iterates such that the kth iterate lies in the space

$$\mathbf{x}^{(0)} + \mathcal{V}_k, \tag{29}$$

with $\mathbf{x}^{(0)}$ the initial guess and

$$\mathcal{V}_k = \operatorname{span}\big\{\mathbf{s}^{(1)}, \mathbf{s}^{(2)}, \ldots, \mathbf{s}^{(k)}\big\}. \tag{30}$$

A natural choice for implementing such iteration is the GCR method, or its older, truncated version known as ORTHOMIN. While the action of the preconditioner P may again be computed efficiently, the standard implementation of the strategy is nevertheless seen to be costly, since the orthogonalization procedure to find the minimal residual solution depends on performing matrix-vector products associated with the large coefficient matrix in (26) and saving large vectors, which give both the search directions and base vectors for expanding the iterated residuals. These full operations can however be avoided if only a part of the preconditioning computations is admitted to be done inexactly.

It turns out that if in the preconditioning the linear solves associated with the coefficient matrices $\mathbf{J}$, $\mathbf{M}_W$, $\mathbf{R}$ and $\mathbf{M}_U$ are always performed accurately (in practice up to an accuracy which is generally desired from the final converged solution), we can accomplish the preconditioned GCR iteration without performing the complete matrix-vector products associated with (26). In addition, the number of vector entries which have to be saved in the computer memory may be reduced significantly. This can be proved by considering the splitting of (27) as

$$\begin{bmatrix} \mathbf{K}_{11} & \mathbf{K}_{12} \\ \mathbf{K}_{21} & \mathbf{K}_{22} \end{bmatrix} \begin{bmatrix} \mathbf{x}_1 \\ \mathbf{x}_2 \end{bmatrix} = \begin{bmatrix} \mathbf{b}_1 \\ \mathbf{b}_2 \end{bmatrix} \tag{31}$$

with $\mathbf{K}_{11} = \mathbf{C}$. If the initial guess is constructed such that

$$\mathbf{K}_{21}\mathbf{x}_1^{(0)} + \mathbf{K}_{22}\mathbf{x}_2^{(0)} = \mathbf{b}_2,$$

then the residual norm corresponding to any solution candidate $\tilde{\mathbf{x}}^{(k)}$ from (29) can be expressed as

$$\|\mathbf{b}_1 - \mathbf{K}_{11}\tilde{\mathbf{x}}_1^{(k)} + \mathbf{K}_{12}\tilde{\mathbf{x}}_2^{(k)}\|$$

for all $k \geq 1$. In effect this observation implies that the optimality criterion associated with solving (26) via the GCR iteration based on the block Gauss-seidel preconditioning can be expressed simply in terms of the matrix blocks $\mathbf{C}$, $\mathbf{D}$ and $\mathbf{L}_U$. In addition, significant savings in the memory usage are possible, since in practice it suffices to characterize the optimal solution in terms of the vector entries which are relevant to computing matrix-vector products with these matrix blocks.

We conclude that, at the cost of performing certain preconditioning computations accurately, the GCR method for (26) based on the block Gauss-Seidel preconditioning can be implemented without assembling the monolithic system in a literal manner. It should be noted that the solution strategy we employ is closely related to the methods already proposed in [13]. We emphasize that a significant gain associated with solving (26) in a fully coupled manner is improved robustness, without a need to find clever strategies for adjusting relaxation parameters. Although the block Gauss-Seidel splitting is generally a rudimentary preconditioning strategy, we see an opportunity for rapid convergence in this connection. We motivate this by the observation already made in Section 2 that, after the change of variables, the coupling occurring via the matrix block $\mathbf{D}$ is weak. It thus appears that the principal problem resolved in the iterative procedure relates to finding the values of $\mathbf{u}$ at the boundary, which is a problem of small order. All computational examples given in the next section support our assertion of rapid convergence.

4. Computational results

We finally describe some additional details regarding how we have implemented the computational methods of Section 3.2 into the open source finite element software Elmer [14]. The utility of the solver is also demonstrated computationally.

4.1. Finite element implementation with a view on parallelism

The actual definition of the coefficient matrices in (26) obviously depends on how finite element spaces $M_h \subset M$, $X_h \subset X$ and $Q_h \subset Q$ for the Galerkin approximation are chosen. Our current implementation is completely based on employing standard approximation spaces as we take $Q_h \subset [H^1(\Omega)]^d \subset Q$.

Using the standard velocity spaces is also convenient from the viewpoint that the linear solves associated with the blocks $\mathbf{M}_W$ and $\mathbf{M}_U$ can then be done sequentially by using the same scalar velocity mass matrix, so that the memory requirements corresponding to the computation of velocity updates become indeed minimal. The other matrices which we assemble are the diagonal blocks $\mathbf{C}$, $\mathbf{J}$ and $\mathbf{R}$ of the preconditioner (28) as well as the interaction blocks $\mathbf{D}$ and $\mathbf{L}_U$ of the coupled system (26), while other computations are performed in a matrix-free manner. We note that in comparison with handling (2) iteratively in combination with a preconditioner based on the approximation of the coefficient matrix in (3), our implementation of the new method necessitates allocating only one additional matrix structure associated with the discretization of a scalar field. This cost can be considered to be minor.

A very appealing feature of the new formulation leading to the discrete problem (26) appears to be that it may enable the approximation by using standard equal-order elements. Considering the requirement of the unique solvability via looking at the homogeneous system associated with (26), we are led to the system

$$\begin{bmatrix} \mathbf{C}_P & -\mathbf{L}_U\mathbf{M}_U^{-1}\mathbf{N} \\ \mathbf{L}_W\mathbf{M}_W^{-1}\mathbf{L}_P & \mathbf{R} \end{bmatrix} \begin{bmatrix} \mathbf{P} \\ \mathbf{Q} \end{bmatrix} = \begin{bmatrix} \mathbf{0} \\ \mathbf{0} \end{bmatrix}, \qquad (32)$$

with $\mathbf{C}_P = \mathbf{C} - \mathbf{D}\mathbf{J}^{-1}\mathbf{E}$ and $\mathbf{L}_P = \mathbf{H}_\theta\mathbf{J}^{-1}\mathbf{E} - \mathbf{H}_P$. Although the standard equal-order approximation may be deficient in the sense that there may be spurious pressure modes $\hat{\mathbf{P}}$ different from the constant approximation such that $\mathbf{L}_P\hat{\mathbf{P}} \approx \mathbf{0}$, the presence of $\mathbf{C}_P$ in (32) is expected to prevent such spurious mode to be a null vector of the homogeneous system. That is, the proposed formulation based on equal-order finite element approximation is expected to be stable without adding a stabilization term.

We do not dwell on the issue of the finite element stability here, but we merely state that all discrete problems (26) were generated in this paper by using standard equal-order elements without seeing any signs of instability in the solutions. In the following, this discretization method based on the piecewise polynomials of degree k is referred to as the HDLinNS(k) approximation (the discrete Helmholtz Decomposition based Linearized Navier–Stokes model). On the other hand, the Galerkin discretization of the original model (1) which is used as reference and obtained by using the velocity and temperature approximations of degree k and the first-degree pressure approximation is referred to as the $P_kP_kP_1$ approximation or $Q_kQ_kQ_1$ approximation when quadrilateral or brick elements are employed. Experimental studies indicate that $P_kP_kP_1$ and $Q_kQ_kQ_1$ schemes satisfy the requirement of finite element stability for all $k \geq 2$; see also [2] where the case $k = 2$ is considered.

The key achievement of the problem reformulation considered is that all subproblem solves which are needed in order to apply the preconditioner are based on the simplified and fairly standard models. As noted already, the velocity updates can be done componentwise, and they are rapidly solvable with standard iterative solvers. The other subsidiary problems requiring effective iterative solvers relate to the models of diffusion and dissipative wave propagation. We expect that the solvers of the discrete diffusion models benefit from the attained scale separation, so that the principal problem there is to find only solution modes which decay quickly as we go away from the boundary. On the other hand, an existing Helmholtz equation solver can be reused in the computation of the pressure update. Taken collectively, we expect that the most demanding subsidiary computations are typically associated with handling the pressure equation and the equation characterizing the vector potential.

Having derived a formulation which is built on basic discrete models, the suitableness of the strategy to utilize parallel computation is also evident. Our platform for implementing the methods described has been the open source software Elmer which supports both serial and parallel computations. It also supports the use of the *hp*-version of the finite element method, so that, in addition to the classic mesh refinement, better resolution may also be sought by increasing the polynomial degree of approximation.

4.2. Monitoring the convergence

As already explained, our implementation of the preconditioned GCR solver for (26) is based on the idea of avoiding the literal assembly of the associated coefficient matrix. Since it is therefore tacit that the block Gauss-Seidel preconditioner is applied accurately except for possibly inaccurate solves of the (1,1) block, the convergence of the GCR iteration may basically be monitored by using the residual norm

$$\left\| \mathbf{D}_C\left(\mathbf{G} - \mathbf{C}\mathbf{P}^{(k)} - \mathbf{D}\boldsymbol{\Theta}^{(k)} - \mathbf{L}_U\mathbf{U}^{(k)}\right) \right\|_\infty, \qquad (33)$$

where $\mathbf{D}_C$ is the diagonal scaling matrix used to equilibrate the first row of the block coefficient matrix in (26). By making a specific choice of how backward error per-

turbations are measured, we then come to bounding the normwise backward error $\eta(\mathbf{x}^{(k)})$ as

$$\begin{aligned}&\eta(\mathbf{x}^{(k)}) \leq \\ &\frac{\|\mathbf{D}_C(\mathbf{G} - \mathbf{C}\mathbf{P}^{(k)} - \mathbf{D}\boldsymbol{\Theta}^{(k)} - \mathbf{L}_U\mathbf{U}^{(k)})\|_\infty}{\|\mathbf{y}^{(k)}\|_\infty + \|\mathbf{D}_C\mathbf{G}\|_\infty} \\ &\leq TOL\end{aligned} \tag{34}$$

where TOL is the stopping tolerance and the vector $\mathbf{y}^{(k)}$ contains the minimum residual iterate values $\mathbf{P}^{(k)}$, $\boldsymbol{\Theta}^{(k)}$ and $\mathbf{U}^{(k)}$ confined to the boundary nodes.

4.3. Computational examples

In the following, two types of computational experiments will be performed. First, we demonstrate the finite element convergence of our HDLinNS(k) approximation as the discretization is refined. Secondly, the performance of the preconditioned GCR solver for the fully coupled discrete problem is considered and its utility for parallel computing is demonstrated. Here we shall focus on the lowest-order case $k = 1$ which may have merit in connection with parallel computing. For example the mass lumping strategy and the related Jacobi preconditioning, which are relevant in connection with performing the velocity updates, may be more effective in the case of low-order discretizations.

In all computations the material is taken to be air at the standard conditions. By expressing all model parameter values in SI units, we thus take $T_0 = 293$, $\rho = 1.21$, $\mu = 1.81 \cdot 10^{-5}$, $\kappa = 0$, $K = 2.6 \cdot 10^{-2}$, $\gamma = 1.4$, and $C_V = 717$. The sound speed c is then defined by the relation $c^2 = \gamma(\gamma-1)C_V T_0$.

4.3.1. Finite element convergence

To begin with, we explore computationally the convergence rate of the HDLinNS(1) approximation in terms of a representative mesh size h. To this end, we consider a straight tube which has the length $L = 0.17$ (m) and a circular cross section of the radius $R = 0.01$ (m). The amplitude of the axial velocity v_z at the other end of the tube is taken to be the real function $v_z = 0.001(1 - r/R)$ (m/s), with r the radial coordinate, while the other tube walls are assumed to be rigid. The frequency is taken to be a resonance value $f = 1000$ (Hz), with $\omega = 2\pi f$. We now handle this problem in two dimensions by exploiting the axial symmetry, so that the computational domain is given by $\Omega = (0, L) \times (0, R)$.

It appears that the accuracy of the discrete pressure solution depends critically on the quality of the edge effect approximation. Therefore we focus here on exploring the asymptotic rate of convergence when the dominant component of error is due to the approximation of the boundary layer. To this end, we use a fine 20×340 mesh of bilinear elements in the interior containing points the distance of which from the wall is not smaller than $\delta = 0.0006$ (m). It can then be verified computationally that the accuracy of HDLinNS(1) solutions is dominated by the discretization error of the boundary layer component for boundary layer meshes which have the edge length $h \gtrsim \delta/20$ in the thickness direction. Such solutions are now compared with the reference solution which is obtained with the hp-version approximation of the standard linearized Navier-Stokes model (1). This model uses the $Q_2Q_2Q_1$ approximation over the interior 20×340 mesh and the high-order $Q_8Q_8Q_1$ approximation in the boundary layer, with two layers of elements in the thickness direction.

Table I. The estimate of the relative L_2 error of the pressure given by the HDLinNS(1) model as the representative mesh size in the boundary layer is taken to be $h = \delta/n$. The number of the preconditioned GCR iterations needed to compute the HDLinNS(1) solution is also shown.

n	$\mathcal{E}_h$	Iterations
4	1.4628e-01	4
6	7.6577e-02	4
8	4.5480e-02	5
12	2.1051e-02	5
16	1.2104e-02	6
20	7.8735e-03	6
24	5.5341e-03	7

The results given in Table I show the estimate of the relative L_2 error of the pressure when the mesh size in the thickness direction varies as $h = \delta/n$, with $4 \leq n \leq 24$. The error is computed as

$$\mathcal{E}_h = \frac{\|p_{\text{ref}} - p_{\text{HDLinNS(1)}}\|_{L_2(\Omega)}}{\|p_{\text{ref}}\|_{L_2(\Omega)}}, \tag{35}$$

where p_{ref} denotes the reference solution based on the hp-approximation of the standard linearized Navier-Stokes model. The results shown indicate that the asymptotic rate of convergence exhibits essentially the optimal behaviour, the error decreasing quadratically as the mesh is refined. The preconditioned GCR iteration counts to obtain the HDLinNS(1) solution are also given in Table I. We see that the preconditioner behaves nearly optimally in this case as the iteration counts depend very mildly on the problem size.

4.3.2. Performance of the preconditioner

The main goal here is to explore in more detail how the performance of the preconditioned GCR solver depends on the problem size. To this end, we consider a tubular Helmholtz resonator model consisting of two cavities and a narrow connecting duct. All these parts have circular cross sections and are placed such that the tube axes form the line of symmetry for the complete system. By using the axial symmetry, the computations may then be performed on the two-dimensional domain $\Omega = (0, R_1) \times (0, L_1) \cup (0, R_2) \times [L_1, L_2] \cup (0, R_3) \times (L_2, L_3)$ where $R_1 = 9.25 \cdot 10^{-3}$, $R_2 = 7.5 \cdot 10^{-4}$ and $R_3 = 5.0 \cdot 10^{-3}$ give the radii of the constituent tubes. In addition, we have $L_1 = 2.5 \cdot 10^{-2}$, $L_2 = 2.9 \cdot 10^{-2}$ and $L_3 = 4.4 \cdot 10^{-2}$. For an illustration of the two-dimensional version of the problem geometry see Figure 1.

The source is defined by prescribing a non-vanishing velocity amplitude on the edge $x_2 = L_3$ where we take

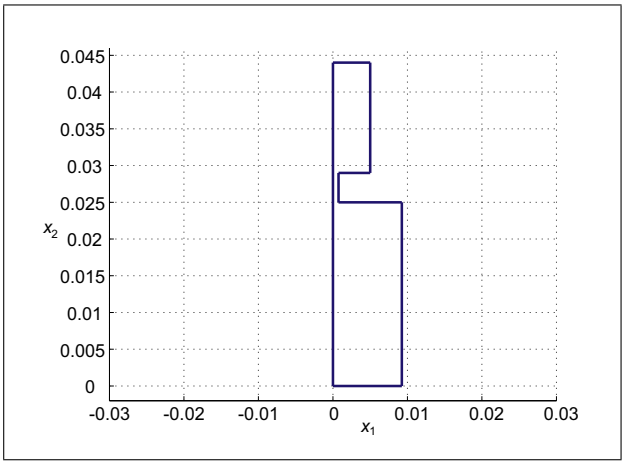

Figure 1. The computational domain for the two-dimensional version of the Helmholtz resonator model.

$v_1(x_1) = 0$ and $v_2(x_1) = J_0(\alpha x_1)$, with J_0 a scaled Bessel function having the maximum value $1.0 \cdot 10^{-3}$. In addition, the scaling factor α is defined such that $\xi = \alpha R_3$ is the first root of $J_0(\xi)$. We also assume that the fluctuation of the temperature vanishes on this edge. On the edge $x_1 = 0$ the symmetry boundary conditions are used, while on the remaining part of the boundary we impose the conventional wall boundary conditions (10) with $\mathbf{g}' = \mathbf{0}$.

Three discretization meshes consisting of linear triangles were created by associating the model boundaries which are different from the symmetry line with an element edge length constraint $h_K = \delta_L$ and allowing the mesh size to increase with a specified grading factor as we go away from these walls. The choices $\delta_L = 5.0 \cdot 10^{-5}, 2.5 \cdot 10^{-5}, 1.25 \cdot 10^{-5}$ then gave us three meshes having the numbers of nodes $n = 16938, 35661, 78117$, with the same numbers of unknowns for approximating a scalar field. In order to explore simultaneously how the iteration counts depend on the frequency, we consider the solutions for three frequencies $f = 500, 1000, 1500$, with $f = 1000$ being close to a resonance frequency of the system. It should be noted that the triangular and tetrahedral meshes employed in this paper are expected to be far from optimal in terms of the number of unknowns. In practice an anisotropic mesh refinement strategy should be used to optimize the discretization size.

The numbers of preconditioned GCR iterations to satisfy the backward error tolerance 10^{-8} are displayed in Table II. Generally we expect that the quality of our initial guess may depend heavily on the frequency, with large errors expected for resonance frequencies (we compute the initial guess by taking $\mathbf{\Theta} = \mathbf{U} = \mathbf{0}$ in the pressure computation). Although there are slight changes in the iteration counts, we see that the iterations converge rapidly for all frequencies. The most challenging problem actually is the solution of the low-frequency response below the resonance frequency. A closer inspection of convergence histories revealed that the slight frequency dependency of iteration counts is primarily explained by the fact that the asymptotic convergence rate may depend to some extent

Table II. The number of preconditioned GCR iterations to solve the axially symmetric Helmholtz resonator model based on the HDLinNS(1) approximation, with n giving the number of nodes.

	$n = 16938$	$n = 35661$	$n = 78117$
$f = 500$	10	16	24
$f = 1000$	10	15	21
$f = 1500$	7	10	16

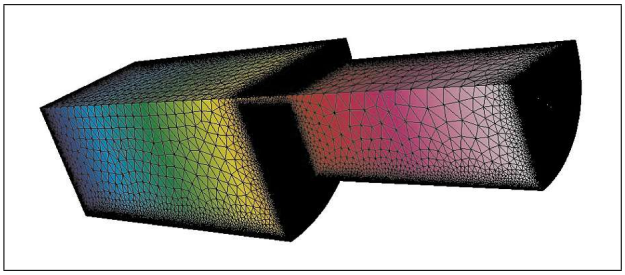

Figure 2. The mesh for the three-dimensional version of the Helmholtz resonator model, with 2,614,773 nodes.

on the model frequency. In view of the results given in Table II, there is a clearer trend that the iteration counts generally increase for larger discretizations of the same case. This may again be explained by a closer observation that the asymptotic convergence rate is not independent of the mesh refinement level. However, we emphasize that even the coarsest mesh here is already fairly fine for practical purposes (cf. the results of Table I showing the relative pressure error 2.11% for $h = 5.0 \cdot 10^{-5}$ at $f = 1000$), so that these iteration counts should give representative examples of the practical performance of the preconditioner. Generally the experiments performed indicate that rapid convergence is obtained by using our preconditioned GCR solver.

4.3.3. The utility for parallel computing

We finally demonstrate the applicability of our solver to handle three-dimensional models of realistic size. In such connection, the use of parallel computing is a typical necessity from the viewpoint of both computer memory usage and a quick evaluation of results.

Here the three-dimensional version of the Helmholtz resonator case described in section 4.3.2 is used as an example. The symmetry conditions are used, so that only a quarter of the complete system is discretized into linear tetrahedra. The boundaries near the narrow duct where the most significant losses are expected to occur is associated with an element size constraint $h_K = 1.8 \cdot 10^{-5}$, whereas a less stringent element size constraint $h_K = 4 \cdot 10^{-5}$ is set on the other solid boundaries. Allowing again the element size to increase as the distance from the solid walls increases, we are then led to a finite element mesh which has 2,614,773 nodes. This mesh is illustrated in Figure 2. We note that using a lowest-order stabilized finite element approximation of the standard model (1) over this mesh would lead to the ten-fold number of real unknowns.

We recall that the key idea in the solver design described has been to obtain a linear solver where even the most demanding parts of computation can be performed by solving simple subsidiary problems. That this goal is essentially achieved here is demonstrated in Table III where we summarize our selection of the iterative solvers which were used to solve the subsidiary problems related to the preconditioning. The simplicity of the equations is highlighted by the fact that the elementary Jacobi preconditioner can be applied widely, the only subproblem for which this strategy is not feasible being the solution of the pressure update characterized by the dissipative wave equation. Although the choices of linear solvers given in Table III demonstrate the obtained ability of producing computational solutions by using standard parallel methods, we emphasize that these choices are by no manner of means expected to be optimal. Optimal complexity and attaining better parallel scalability should generally be sought by considering other linear solvers for the subsidiary problems, but we leave this as a subject for future research.

The three-dimensional example computations were performed in parallel by using 256 processors. The results were computed for 41 sample frequencies $f = f_i \in [900, 1100]$ near the resonance value. For comparison the same case was also solved using the axially symmetric version of the HDLinNS(1) model on the finest triangular mesh (with 78117 nodes) used in the experiments of Section 4.3.2. In addition, to obtain a reference solution, the same problem was solved using the axially symmetric $Q_2Q_2Q_1$ discretization of the standard linearized Navier-Stokes model (1) on a carefully refined mesh. The accuracy of this reference solution was verified by considering the effect of further mesh refinement.

We note that in the case of the three-dimensional HDLinNS(1) model the average count of the preconditioned GCR iterations to obtain the solution having the backward error smaller than 10^{-9} was found to be 19, so that quick convergence was again attained. These iteration counts were also found to be comparable with those obtained in the corresponding two-dimensional simulation.

The computed results are finally illustrated in Figure 3 where we show the averages of the real and imaginary parts of the pressure amplitude computed as

$$\frac{\int_S \Re e[p]\,\mathrm{d}S}{\int_S \mathrm{d}S} \quad \text{and} \quad \frac{\int_S \Im m[p]\,\mathrm{d}S}{\int_S \mathrm{d}S}$$

over the boundary S where the velocity source is specified (the end at $x_2 = L_3$). We see that the results are in good agreement. We note that the axially symmetric version of HDLinNS(1) model is based on finer resolution and, as expected, produces a slightly better agreement with the reference solution.

5. Concluding remarks

The computational experiments given in this paper demonstrate that the proposed discrete Navier–Stokes model based on the Helmholtz decomposition exhibits optimal accuracy and, most importantly, admits the solution by the block preconditioned iteration method which may be handled without difficulty in a parallel computer. As a result, the performance acceleration of the proposed method can be sought by focusing on auxiliary solvers for handling fairly elementary models. The most important of them are the viscous version of the Helmholtz model and the homogeneous diffusion equations for a complex scalar field and a complex vector potential.

Table III. The summary of iterative solvers used for the preconditioning computations in the case of three-dimensional version of the Helmholtz resonator case.

Block	Linear solver	Preconditioner
C	BiCGStabL(4)	parallel ILU(0)
J	GCR(20)	Jacobi
$\mathbf{M}_W/\mathbf{M}_U$	GCR(50)	Jacobi
R	GCR(100)	Jacobi

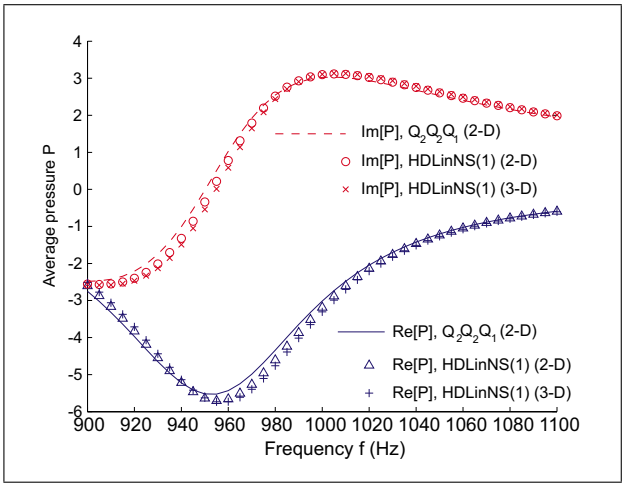

Figure 3. The averages of the real and imaginary parts of pressure amplitude over the end where the source is given in the case of the Helmholtz resonator problem. The reference solution is based on the axially symmetric $Q_2Q_2Q_1$ discretization in two dimensions. The results for the axially symmetric version of HDLinNS(1) model (with 78,117 nodes) and the three-dimensional HDLinNS(1) model (with 2,614,773 nodes) are also shown.

Acknowledgement

The research of this paper was funded by Nokia Corporation.

References

[1] M. Malinen, M. Lyly, P. Råback, A. Kärkkäinen, L. Kärkkäinen: A finite element method for the modeling of thermo-viscous effects in acoustics. – In: Proceedings of the 4th European Congress on Computational Methods in Applied Sciences and Engineering. P. Neittaanmäki, T. Rossi, K. Majava, O. Pironneau (eds.). University of Jyväskylä, 2004.

[2] W. R. Kampinga, Y. H. Wijnant, A. de Boer: Performance of several viscothermal acoustic finite elements. Acta Acustica united with Acustica **96** (2010) 115–124.

[3] N. Joly: Finite element modeling of thermoviscous acoustics on adapted anisotropic meshes: Implementation of the particle velocity and temperature variation formulation. Acta Acustica united with Acustica **96** (2010) 102–114.

[4] R. Christensen: Modeling the effects of viscosity and thermal conduction on acoustic propagation in rigid tubes with various cross-sectional shapes. Acta Acustica united with Acustica **97** (2011) 193–201.

[5] W. R. Kampinga: Viscothermal acoustics using finite elements. Analysis tools for engineers. PhD. thesis, University of Twente, 2010.

[6] M. J. J. Nijhof: Viscothermal wave propagation. PhD. thesis, University of Twente, 2010.

[7] M. Benzi, G. H. Golub, J. Liesen: Numerical solution of saddle point problems. Acta Numer. **14** (2005) 1–137.

[8] M. Malinen: Boundary conditions in the schur complement preconditioning of dissipative acoustic equations. SIAM J. Sci. Comput. **29** (2007) 1567–1592.

[9] P. M. Morse, K. U. Ingard: Theoretical acoustics. Princeton University Press, Princeton, 1986.

[10] E. Dokumaci: An integral equation formulation for boundary element analysis of acoustic radiation problems in viscous fluids. J. Sound Vib. **147** (1991) 335–348.

[11] C. Karra, M. Ben Tahar: An integral equation formulation for boundary element analysis of propagation in viscothermal fluids. J. Acoust. Soc. Am. **102** (1997) 1311–1318.

[12] W. R. Kampinga, Y. H. Wijnant, A. de Boer: An efficient finite element model for viscothermal acoustics. Acta Acustica united with Acustica **97** (2011) 618–631.

[13] K. Ito, J. Toivanen: Preconditioned iterative methods on sparse subspaces. Appl. Math. Lett. **19** (2006) 1191–1197.

[14] Elmer finite element software homepage, http://www.csc.fi/elmer.